# SEM observation and Raman analysis on 6H–SiC wafer damage irradiated by nanosecond pulsed Nd:YAG laser

**Zhiyu Zhang (张志宇)[1*], Yang Xu (杨 旭)[2], and Binzhi Zhang (张斌智)[1]**

[1]*Changchun Institute of Optics, Fine Mechanics and Physics, Chinese Academy of Science, Changchun 130033, China*

[2]*Jilin University, Changchun 130025, China*

**Corresponding author: zhangzhiyu@ciomp.ac.cn*

Received April 7, 2014; accepted July 16, 2014; posted online January 26, 2015

Silicon carbide (SiC) is a wide bandgap semiconductor which exhibits outstanding mechanical, chemical properties, and potential for a wide range of applications. Laser technology is being established as an indispensable powerful tool to induce structural or morphological modifications on hard brittle materials. SiC (6H–SiC wafer) is irradiated by nanosecond pulsed Nd:YAG laser to evaluate microstructure and mechanical properties of irradiation areas. Raman spectroscopy analysis reveals that irradiations produce homonuclear Si–Si bonds and disordered phase of crystalline SiC. Crystal structure changes are observed as a consequence of laser-induced melting and resolidification. Hardness in the irradiation area exhibits a significant decrease. The formation of silicon film facilitates material removal rate, surface electrical conductivity, and ceramics conjunction.

*OCIS codes: 220.1920, 220.4610.*
*doi: 10.3788/COL201513.S12203.*

Owing to its excellent electrical, physical, chemical as well as mechanical properties, silicon carbide (SiC) is also expected to serve as the next generation material for high temperature, high frequency, high power, and energy-saving electronics applications, which are currently even impossible or unaffordable using Si, Ge, or GaAs-based devices[1–5]. In recent years, as the cost of SiC wafer continues to decrease and its size continues to increase, use of SiC wafer in microelectromechanical systems becomes more and more attractive. Nevertheless, from the micromachining point of view, SiC is well-known for its poor machinability for defect-free substrate planarization. Herein, fabrication of micromachined structures on SiC wafer using the conventional bulk micromaching techniques has proven to be impossible in most cases. This is one of the biggest obstacles for the commercialization of SiC substrate devices. Fortunately, in the micromanufacturing industry, laser technology is being established as a promising powerful tool to induce structural or morphological modifications in the near-surface region on hard and brittle semiconductor materials. Femtosecond (fs) pulsed lasers are recently researched by many groups as it can fabricate nearly all types of solid materials because of its unique characteristics of ultra-short pulse width which is shorter than the temperature transfer time from electrons to the lattice[6], leading to a sublimate removal material and leaving negligible thermal damage on the substrate. Although fs lasers really have high capacity on the microstructure machining, such as recently reported channels on microfluid control devices, grating, and even lens, fs lasers have several disadvantages for practical use, due to high cost but small pulse energy as well as instability. As a common realization, nanosecond laser is not well suited for precise microstructuring due to thermal or mechanical damages, such as no good edge quality, recast layers, burrs, and cracks, whereas it can only be used for microdrilling and marking of semiconductors or metals. Based on the available references, corresponding studies have performed on bulk single-crystal wafer by nanosecond laser limited to following summary. Fedorenko *et al.*[7], using 340 nm N2 laser and 1064/532 nm YAG laser, examined structural and morphological changes in the near-surface layer and on the surface of 6H–SiC in the range of laser intensities insufficient to cause visually observable changes on the surface. Nanostructures having a shape of a hill arising along the circular line around the focused spot were obtained. In their work, the micrometer range structures were not reported, which is common in the usual applications. Wernicke *et al.*[8] obtained through-wafer micro holes with a diameter of 50–100 mm in 400 mm thick bulk 4H–SiC by a frequency-tripled solid-state laser (355 nm) with a pulse width of 30 ns and a focal spot size of 15 $\mu$m. However, the critical value was not said clearly. Zoppel *et al.*[9] studied laser ablation of bulk single crystal 3C–SiC with emphasis on the influence of pulse duration and laser wavelength. Experiments with 193 and 248 nm excimer nanosecond lasers have been carried out. The nanowavelength effects cannot be found in their articles. However, these have not yet been investigated in sufficient depth and extent up to now.

 © 2015 Chinese Optics Letters

Fig. 1. Nd:YAG laser machining system.

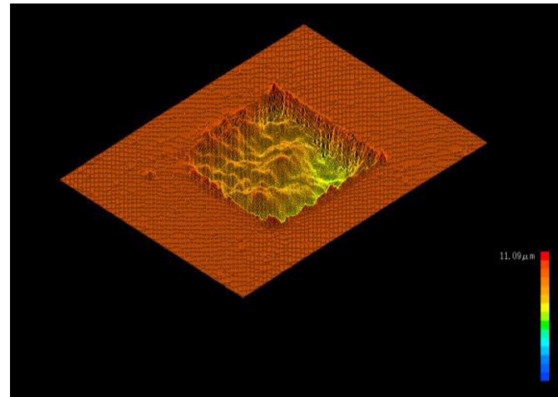

Fig. 2. Picture of irradiation area (up-down view).

Although there are several studies on nanosecond laser irradiation on SiC wafer, there is still a lack of detailed technical data on structural, chemical, and especially mechanical properties such as hardness and fracture changes in irradiated area. In order to get more insight into the laser–material interaction, nanosecond pulsed Nd:YAG laser is chosen to ablate single-crystalline 6H–SiC wafer surface. Crystal structural change is investigated by Raman spectroscopy. Results are discussed according to previous results and perspectives presented in term of further mechanical characterizations.

The experiments were carried out at room temperature and atmospheric pressure. In this experiment, the 6H–SiC single-crystal wafer (Cree, Inc.) with a typical diameter of 50.8 mm (2″) and thickness of 234.0 $\mu$m was considered. Before laser ablation, 6H–SiC wafer was cleaned in an acetone ultrasonic bath for 15 min and dried on heat plate. Next, the 6H–SiC wafer was mounted on a three-axis stage and irradiated by the QuikLaze-50 Nd:YAG laser machining system (New Wave Research, Inc.). This laser system is shown in Fig. 1 with an $XY$ aperture to shape the laser beam spot as rectangular, with the adjustable spot area of 1×1–50×50 ($\mu$m). The output energy per pulse was determined by a pyroelectric detector. The pulse repetition rate could be varied from 1 to 50 Hz. Therefore, the single- and multi-pulse modes could be used. This system allowed to micromachine materials by ablation with minimal thermal effect thanks to a short pulse width of 3–4 ns. Moreover, during laser irradiation, the instant change in the surface could be motivated from a cathode ray tube screen connected to the laser machine with a magnification of 1000×. In the experiment, the $XY$ apertures were both set to 20%, enabling a 50×50 ($\mu$m) square irradiation area. The incident laser beam was perpendicular to the irradiated surface. Table 1 shows the laser processing parameters.

**Table 1.** Laser Processing Parameters

| **Machine** | **QuikLaze-50** |
|---|---|
| Workpiece | 6H–SiC wafer |
| Wavelength | 355 nm |
| Pulse time | 3–4 ns |
| Irradiation energy density | 0.20–0.60 J/cm$^2$ |
| Irradiation times | 1–20 |
| Irradiation area | 60×60 ($\mu$m) |

After irradiation, a scanning electron microscope (SEM) was used to study the laser ablation regime. The sample was also observed with a Mitaka to examine the profile of the irradiated area. In order to study the crystalline crystal structural changes, the laser processed areas were examined using a laser micro-Raman spectroscope (NRS-3100, JASCO Corporation, Japan). The wavelength of the laser was 532 nm and the focused laser spot size was 1 $\mu$m. In addition, a nanoindentation tester (ENT-1100a, Elionix Co. Ltd.) was used for analyzing the surface hardness on both irradiation and unirradiation zones.

Figure 2 shows a picture of the irradiation area with laser wavelength of 355 nm for 10 pulses, obtained by using a laser microscope. Figure 3 shows the side-view photo of the abovementioned irradiated area. Figure 4 shows the measured surface profile. The peak-to-valley

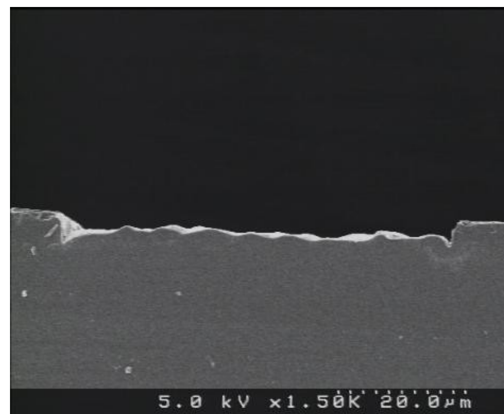


Fig. 3. SEM picture of irradiation area (side view).

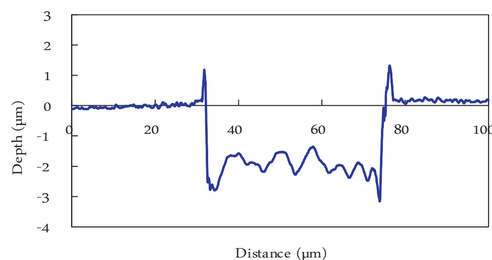


Fig. 4. Surface profile of irradiation area.

roughness is about 150–200 nm and presents smooth, rounded hillocks rather than regular sharp edges. This may indicate that the 6H–SiC surface has re-melted during the laser pulse. The ablation mechanism for the formation of holes is discussed in Ref. [10].

The laser–material interaction is with a strong dependence on the bandgap energy of the material[11]. The 355 nm wavelength is larger because of the higher absorption coefficient of SiC in the ultraviolet spectrum. For the ablation of SiC with 532 nm laser, higher intensity is required compared with the 355 nm laser. This is because the bandgap energy of SiC is around 3.0 eV and the electron affinity is around 4.0 eV, which makes the minimum energy required for bond breakage near 7.0 eV. The photo energies of the 355 and 532 nm wavelengths are approximately 3.49 and 2.32 eV, respectively. Therefore, in order to break the bonds using these wavelengths, the interaction has to be a multi-photon process.

Figure 5 shows the unirradiated sample spectra with four-single strong peaks at 154, 767, 788, and 964 $cm^{-1}$, which correspond to peaks from crystalline $\alpha$-SiC 6H polytype[12]. Figure 6 shows the second Raman peaks which are at 1504 and 1703 $cm^{-1}$ with furrow features. Figures 7 and 8 show the corresponding Raman peaks after irradiation. A decrease in intensity and broadening of the crystalline SiC peaks are observed after irradiation. Figure 7 shows a sharp peak at ~500 $cm^{-1}$ representing crystalline silicon (Si–Si homonuclear bonds). However, the Raman peaks did not show a weak broad

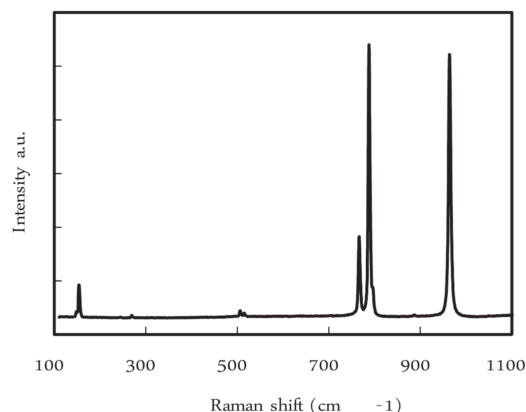


Fig. 5. First Raman spectra on unirradiated sample.

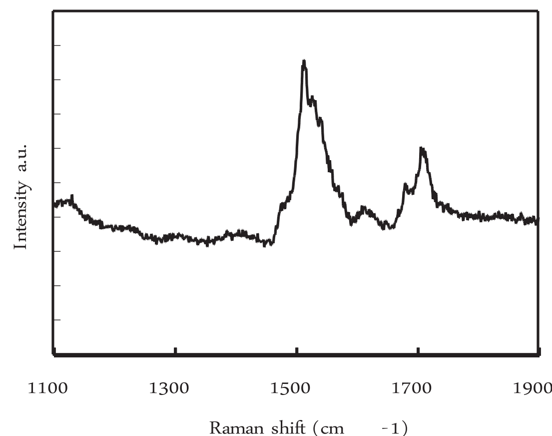


Fig. 6. Second Raman spectra on unirradiated sample.

peak around 480 $cm^{-1}$, which indicates the existence of amorphous silicon. Furthermore, the broad peak around 300 $cm^{-1}$ attributed to the SiC disordered. The peak around 800 $cm^{-1}$ is attributed to highly disordered SiC.

It is well-known that the liquid phase of SiC does not exist under equilibrium conditions[13]. However, according to Scace and Slack[14], SiC was able to decompose without congruent melting, resulting in a silicon rich liquid in equilibrium with graphite at temperatures from 2830 to 3160 °C. When the liquid resulting from the decomposition of SiC is cooled below the decomposition temperature, Si reacts with the dissolved and suspended carbon to form the cubic SiC. In Raman experiment, however, no cubic SiC peak is detected. The existence of nanocrystalline Si indicates that SiC decomposed to Si and C. The resolidified melt remained nanocrystalline and amorphous silicon, the same as the crystallization when laser processes the high hydrostatic machining-induced amorphous surface. In Fig. 8, it can be seen that a furrow features between 1100 and 1900 $cm^{-1}$ and there is no nanocrystalline graphite at 1608 and 1357 $cm^{-1}$, which indicate the existence of nanocrystalline graphite, while there is only a wide broad peak around 1300–1700 $cm^{-1}$.

Figures 9 and 10 show the SEM photos of the nanoindentation tests on the unirradiated and irradiated areas

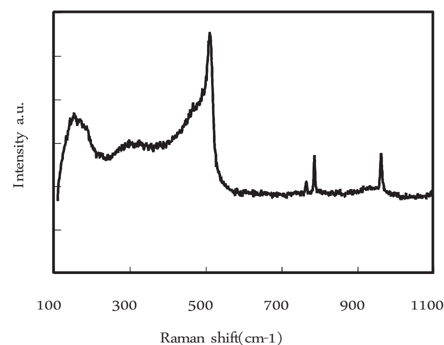


Fig. 7. First Raman spectra on irradiated sample.

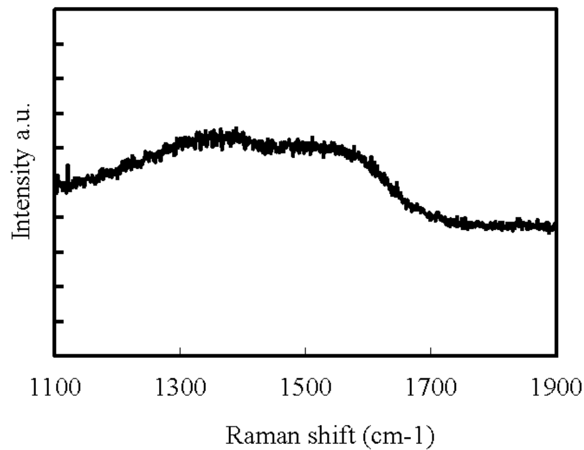


Fig. 8. Second Raman spectra on irradiated sample.

of SiC wafer, respectively. It is clearly seen that the nanoindent on the irradiated one shows significant ductility, which indicates that the irradiated surface has different material properties compared with the unirradiated area. The softer irradiated area can facilitate the mechanical removal. Thus, it can be an effective method to generate the smooth SiC surface by machining the irradiated surface.

Results show that the irradiation produced a chemical decomposition on the treated areas leading to an enrichment of silicon on the surface. As for mechanically smoothing SiC substrate, the material removal rate can be significantly increased because silicon is far softer than SiC. Moreover, the formation of silicon rich surface film where the silicon is predominant allows to develop conducting regions on the surface. In addition, these may be used for joining ceramics to each other or with metal.

In conclusion, this work gives us more insight into the laser–material interaction between the nanosecond pulsed Nd:YAG laser and single-crystalline 6H–SiC wafer surface. Crystal structural changes are investigated by

Fig. 9. Microindent on unirradiated area on SiC wafer.

Fig. 10. Microindent on irradiated area on SiC wafer.

SEM observation, Raman spectroscopy, and nanoindentation. Raman spectroscopy analysis reveals that irradiations produced homonuclear Si–Si bonds and disordered phase of crystalline SiC. Crystal structure changes are observed as a consequence of laser-induced melting and resolidification. Hardness in the irradiation area exhibits a significant decrease. The formation of silicon-film facilitates material removal rate, surface electrical conductivity, and ceramics conjunction.

This work was supported by the National Natural Science Foundation of China under Grant No. 51305422.

## References

1. Y. Dai, H. Ohmori, W. Lin, H. Eto, N. Ebizuka, and K. Tsuno, Key Eng. Mater. **291–292,** 121 (2005).
2. H. Cheng, Z. Feng, S. Lei, and Y. Wang, Mater. Manuf. Processes **20,** 917 (2005).
3. H. Kitahara, Y. Noda, F. Yoshida, H. Nakashima, N. Shinohara, and H. Abe, J. Ceram. Soc. Jpn. **109,** 602 (2001).
4. Zhang, J. Yu, and Z. Zhang, Proc. SPIE **2861,** 296 (1996).
5. R. N. Wilson, *Reflecting Telescope Optics II: Manufacture, Testing, Alignment, Modern Techniques* (Springer-Verlag, 2002).
6. X. Tonnellier, P. Morantz, P. Shore, and P. Comley, Proc. SPIE **7739,** 773905 (2010).
7. L. Fedorenko, A. Medvid, M. Yusupov, V. Yukhimchuck, S. Krylyuk, and A. Evtukh, Appl. Surf. Sci. **254,** 2031 (2008).
8. T. Wernicke, O. Kruger, M. Herms, J. Wurfl, H. Kirmse, W. Neumann, T. Behm, G. Irmer, and G. Trankle, Appl. Surf. Sci. **253,** 8008 (2007).
9. S. Zoppel, M. Farsari, and R. Merz, Microelectron. Eng. **83,** 1400 (2006).
10. H. Suzuki, S. Kodera, S. Maekawa, N. Morita, E. Sakurai, and K. Tanaka, Int. J. Jpn. Soc. Precis. Eng. **64,** 619 (1998).
11. Y. E. Tohme, Proc. SPIE **6462,** 64620K (2007).
12. Q. Wang, W. Cong, Z. Pei, H. Gao, and R. Kang, J. Manuf. Process. **11,** 66 (2009).
13. Y. Wu, S. Yokoyama, T. Sato, W. Lin, and T. Tachibana, Int. J. Mach. Tool Manuf. **49,** 933 (2009).
14. I. Scace and G. Slack, J. Chem. Phys. 30, 1551 (1959).